Angle dependence of the ferromagnetic resonance linewidth in easy-axis and easy-plane single crystal hexagonal ferrite disks

M. J. Hurben,[a] D. R. Franklin,[b] and C. E. Patton
Department of Physics, Colorado State University, Fort Collins, Colorado 80523

(Received 26 July 1996; accepted for publication 2 February 1997)

Ferromagnetic resonance measurements were made as a function of the static external field angle for *c*-plane disks of single crystal flux grown manganese substituted barium *M*-type (Ba-*M*) and zinc *Y*-type (Zn-*Y*) hexagonal ferrites at 50 and 8.8 GHz, respectively. A shorted waveguide technique was used. Analysis of the FMR field versus angle results confirmed the operational assumption of a uniform mode response. For the easy-axis Ba-*M* disk, the linewidth was 69 Oe when the external field and magnetization vectors were perpendicular to the disk. The linewidth increased to a maximum measured value of 472 Oe when the magnetization was directed 45.4° from the sample normal. For the easy-plane Zn-*Y* disk, the linewidth had a minimum value of 18 Oe when the field and magnetization vectors were in-plane. The maximum linewidth was 391 Oe when the magnetization was directed 25.2° from the disk normal. The linewidths were larger than predicted for reasonable values of the Landau–Lifshitz damping and showed angle dependences which indicated nonintrinsic contributions to the loss. A modified two magnon scattering calculation based on the model of Sparks, Loudon, and Kittel was used to investigate these linewidth differences. The calculation included anisotropy modifications to the spin wave band for each material. The angle dependences of the excess linewidths show qualitative agreement with the two magnon predictions, with inhomogeneity sizes on the order of 1 and 0.25 μm and volume fractions of 0.01 and 0.005 for the Ba-*M* and Zn-*Y* disks, respectively. © *1997 American Institute of Physics.* [S0021-8979(97)01010-4]

I. INTRODUCTION

Because of their large anisotropy, hexagonal ferrites are ideally suited for millimeter wave device applications. Such uses, however, will require much lower losses than found in present materials. High field effective linewidth and ferromagnetic resonance linewidth measurements of single crystal barium ferrite (Ba-*M*) indicate that these losses may be partly attributed to an inhomogeneity related two magnon scattering contribution.[1]

One measurement which may help clarify the two magnon contribution to the linewidth in thin disk samples is the dependence of the linewidth on the external static field orientation. If the angle between the external static field and the sample normal is varied, the position of the spin wave manifold is shifted relative to the FMR frequency. The number of degenerate spin waves to which the uniform mode can couple in the two magnon process, and hence the linewidth, will change accordingly. As a result, the linewidth as a function of field orientation will reflect the presence of two magnon scattering and may help characterize the microstructure related contribution to the loss.[2] The angle dependence may be particularly useful for highly anisotropic materials because of the significant modification of the spin wave band and the effect of this modification on the scattering.

In this work, the angle dependences of the FMR fields and linewidths in both easy-axis Ba-*M* and easy-plane zinc *Y*-type (Zn-*Y*) single crystal flux grown hexagonal ferrite *c*-plane disks were measured at fixed frequency. These fields and linewidths were then compared with theoretical predictions based on a uniform mode response and constant Landau–Lifshitz (L–L) damping. The FMR field versus angle results confirm the operational assumption of a uniform mode response. The measured linewidths, however, were generally higher than predicted for reasonable values of the L–L damping and showed angle dependences which indicated nonintrinsic contributions to the loss.

The differences between the measured linewidths and the calculated L–L linewidths as a function of orientation were investigated in terms of an inhomogeneity induced two magnon scattering mechanism. The two magnon calculation follows the work of Sparks, Loudon, and Kittel (SLK)[3] and is based on the transition probabilities for scattering of the uniform precession to degenerate spin waves due to magnetic inhomogeneities in the material. Two different approaches were used. The first approach, termed ''spherical void scattering,'' is based on the original SLK formalism. In this case, the coupling between the uniform mode and the degenerate spin waves is a strong function of the spin wave propagation direction. For the second approach, termed ''isotropic scattering,'' the coupling is assumed to be independent of the spin wave propagation direction. The resulting angle dependence of the two magnon linewidth will reflect the choice of the scattering model as well as the spin wave band modifications.

The results of the calculations indicate that inhomogeneity related two magnon scattering losses are significant in flux grown hexagonal ferrite materials. For the Ba-*M* case, the excess linewidth shows the best agreement with the two magnon theory for isotropic scattering from inhomogeneities

[a]Electronic mail: hurbenm@titan.ds.boeing.com
[b]Permanent Address: School of Chemistry, Physics and Radiography, University of Portsmouth, Hampshire, PO1 2DZ, Great Britain.

 0021-8979/97/81(11)/7458/10/$10.00 © 1997 American Institute of Physics

on the order of 1 μm, which is the size of the voids observed by scanning electron microscopy (SEM) in Ba-M single crystals.[4] For the Zn-Y case, the excess linewidth shows best agreement with the spherical void model and 0.25 μm scatterers.

II. FMR MEASUREMENT AND ANALYSIS

A. Experiment

The bulk single crystal materials used in this study were high purity manganese substituted Ba-M hexagonal ferrite, $BaFe_{12-x}Mn_xO_{19}$ with $x=0.1$, and Zn-Y hexagonal ferrite, $Ba_2Mn_{.68}Zn_{1.82}Fe_{11.83}O_{21.2}$. The manganese substitution serves to compensate for excess Fe^{2+} content and reduce conductivity and the associated eddy current loss. Both materials posses a uniaxial anisotropy. For the Ba-M sample, the easy direction is along the c-axis, while the Zn-Y sample exhibits an easy c-plane.

The single crystals were prepared at Purdue University by standard flux-melt growth methods.[4] Single crystal c-plane platelets were cut and polished to the shape of thin disks using standard lapidary techniques. The diameters were 1.07 and 1.4 mm, and the thicknesses were 0.076 and 0.15 mm for the Ba-M and Zn-Y samples, respectively. The demagnetizing factor perpendicular to the disk plane N_Z was 0.897 for the Ba-M disk and 0.852 for the Zn-Y disk, as calculated by the Osborn method.[5] Vibrating sample magnetometry (VSM) yielded $4\pi M_s$ values of 4.6 ± 0.1 kG for the Ba-M disk and 2.3 ± 0.1 kG for the Zn-Y disk. The effective anisotropy field H_A was also determined from VSM measurements in terms of the saturation field $H_{\rm SAT}$ required to saturate the Ba-M disk in the hard c-plane or the Zn-Y disk along the hard c-axis. The H_A values were determined according to $|H_A|=H_{\rm SAT}-4\pi M_s N$, where N is the demagnetizing factor along the direction of the saturating field. The measurements yielded H_A values of 16.3 ± 0.1 kOe for the Ba-M disk and -9.5 ± 0.2 kOe for the Zn-Y disk. The negative value of H_A for the Zn-Y sample reflects the easy-plane character of the anisotropy.

The FMR field and half-power linewidth were measured by a standard shorted waveguide technique.[6] The measurement frequency was 50 GHz for the Ba-M disk and 8.8 GHz for the Zn-Y disk. The samples were mounted on the side of a TE_{10} waveguide short, one-quarter wavelength from the short. The microwave field was in the disk plane and perpendicular to the applied static field. The incident microwave power level was 1.0 mW. The spectrometer system consisted of a Varian V-4012 electromagnet and V-FR2803 power supply controlled by a Micro-Now 8320A field controller and an F. W. Bell 9900 Gaussmeter. The maximum static field available was approximately 22 kOe. The microwave signal was generated with a Hewlett–Packard (H–P) 8341B synthesized sweeper and H–P 8349B microwave amplifier and analyzed with a H–P 8757A scalar network analyzer.

The sample and magnetic field geometry at static equilibrium is illustrated schematically in Fig. 1. The sample is oriented relative to some right-handed X-Y-Z frame such that the sample normal is parallel to the Z-axis. This direction also corresponds to the uniaxial crystalline c-axis. A

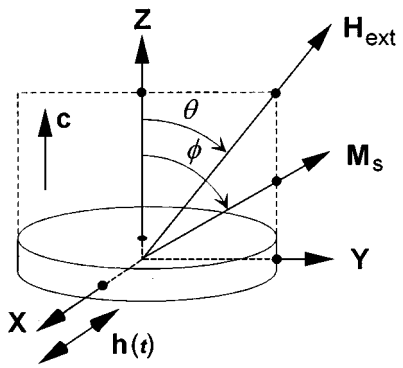

FIG. 1. Disk, field, and static magnetization geometry for the FMR measurements. The external field $\mathbf{H}_{\rm ext}$ is applied at an angle θ relative to the sample normal and crystalline c-axis and lies in the Y-Z plane. The static magnetization $\mathbf{M}_s$ lies in the Y-Z plane at an angle ϕ relative to the Z-axis. The microwave field $\mathbf{h}(t)$ is applied along the X-axis.

static external magnetic field $\mathbf{H}_{\rm ext}$ is applied at an angle θ relative to the sample normal and is taken to lie in the Y-Z plane. The static magnetization vector $\mathbf{M}_s$ also lies in the Y-Z plane and is directed at an angle ϕ relative to the sample normal. The microwave magnetic field $\mathbf{h}(t)$ is applied in the plane of the disk, along the X-axis. This configuration ensures that the microwave field remains perpendicular to the static field and magnetization vectors as the angle θ is varied.

The specific situation in Fig. 1 could apply to an isotropic material, an easy-plane material, or an easy-axis material with $H_A<4\pi M_s$. For a Ba-M disk with easy-axis anisotropy and $H_A>4\pi M_s$, the magnetization angle ϕ will be smaller than the field angle θ. The condition for static equilibrium, namely, a net torque of zero on $\mathbf{M}_s$, yields an expression which relates the field and magnetization angles θ and ϕ.

$$4H_{\rm ext}\sin(\theta-\phi)=[4\pi M_s(1-3N_Z)+2H_A]\sin(2\phi). \tag{1}$$

For $H_{\rm ext}>|H_A|$, the field and magnetization vectors will be parallel with $\mathbf{H}_{\rm ext}$ applied either perpendicular to the disk, where $\phi=\theta=0°$, or in-plane, with $\phi=\theta=90°$.

In the experiment, the angle θ was varied by rotation of the electromagnet about the shorted waveguide containing the sample. FMR profiles for the Ba-M disk were taken in θ steps of 2° up to a maximum angle of 70° relative to the sample normal. At larger angles, additional magnetostatic mode resonances produced spectra which were too complicated to analyze in terms of a simple FMR response. For the Zn-Y disk, the fields and linewidths vary rapidly with external field angle for small values of θ, due to the combined effects of anisotropy and demagnetization. For this reason, it was preferable to measure the field and linewidth in approximately 2° steps of the magnetization angle ϕ. Equation (1) was used to estimate the θ values which corresponded to this step size. These θ step sizes ranged from about 0.4° close to $\theta=0°$ to about 10° close to $\theta=90°$.

B. Uniform mode analysis

In principle, there are two ways to perform a FMR experiment. In the first approach, the operating frequency and field orientation angle are held fixed at ω and θ, respectively, while the strength of the external field $\mathbf{H}_{\text{ext}}$ is varied. The response is then characterized by the FMR field H_0 and field linewidth ΔH. The field H_0 is defined to be the value of H_{ext} for maximum microwave power absorption. The linewidth ΔH is the interval in field units between the half-power points. This is the standard experimental approach and was used in this study.

In the second approach, which is important for theoretical considerations, the static field $\mathbf{H}_{\text{ext}}$ is applied at some angle θ and held at a fixed strength while the operating frequency ω is varied. The response is then characterized by the FMR frequency ω_0 for a maximum power absorption and the frequency linewidth $\Delta\omega$. This linewidth is the interval, in frequency units, between the half-power points of the absorption profile and is conveniently expressed in terms of magnetic field units as $\Delta(\omega/\gamma)$.

The objective of the uniform mode analysis which follows is to determine the FMR response in terms of the field parameters H_0 and ΔH for a given external field orientation. The analysis yields relatively simple working expressions for the FMR frequency ω_0 and frequency linewidth $\Delta(\omega/\gamma)$, but can also be solved to determine the field parameters H_0 and ΔH. Damping is introduced in a phenomenological manner in terms of both the L–L and Bloch–Bloembergen (B–B) formalisms. The L–L formalism is used to account for the overall intrinsic contribution to the loss. The B–B model is used for the two magnon contribution because the L–L damping model is not physically consistent with the two magnon process.[7] These models lead to different linewidth expressions which are discussed shortly.

The results from the uniform mode analysis will first be used to analyze the measured dependence of the FMR field H_0 on the field angle θ. Material parameters such as H_A, $4\pi M_g$, and γ can be determined by fitting the theoretical H_0 versus θ curves to the experimental results. The experimental linewidths ΔH will then be compared to the intrinsic linewidths predicted for L–L damping alone. The nonintrinsic portion of the linewidth will then be found by subtracting the estimated L–L contribution from the data.

The analysis begins with a modified torque equation of motion for the magnetization vector $\mathbf{M}(t)$, which is taken to consist of the static component $\mathbf{M}_s$ and a small dynamic component $\mathbf{m}(t)$ perpendicular to $\mathbf{M}_s$. If the longitudinal relaxation is neglected, the modified torque equation is

$$\frac{d\mathbf{m}(t)}{dt} = -\gamma\mathbf{M}(t)\times\mathbf{H}(t) - \lambda\,\frac{\mathbf{M}(t)}{M_s^2}\times[\mathbf{M}(t)\times\mathbf{H}(t)] - \frac{\mathbf{m}(t)}{2T}. \tag{2}$$

Here, $\mathbf{H}(t)$ represents the total effective magnetic field in the sample, γ is the gyromagnetic ratio, λ is the L–L relaxation rate, and T is the B–B relaxation time for the energy associated with the dynamic magnetization. The gyromagnetic ratio γ has a typical value of 2.8 GHz/kOe for these ferrite materials.[8] A typical linewidth on the order of 50 Oe for a Ba-M sample at 50 GHz would correspond to a λ value of 1×10^7 rad/s or a $1/T$ value of 1×10^9 rad/s.

In the usual uniform mode analysis, the dynamic component $\mathbf{m}(t)$ is assumed to have a magnitude much less than M_s and to have an $e^{i\omega t}$ dependence. This leads to an expression for ω_0,

$$\omega_0 = \gamma\sqrt{H_x H_y}. \tag{3}$$

The H_x and H_y represent two stiffness fields given by

$$H_x = H_{\text{ext}}\cos(\theta-\phi) + \frac{1}{2}[2H_A - 4\pi M_s \times(3N_Z-1)]\cos^2\phi \tag{4}$$

and

$$H_y = H_{\text{ext}}\cos(\theta-\phi) + \frac{1}{2}[2H_A - 4\pi M_s \times(3N_Z-1)]\cos(2\phi). \tag{5}$$

The H_x and H_y parameters are effective stiffness fields which characterize the instantaneous torque exerted on $\mathbf{M}(t)$ when it is tipped parallel to the $\mathbf{h}(t)$ direction or perpendicular to the $\mathbf{h}(t)$ direction, respectively.

The above results provide a relatively simple working expression for ω_0 as a function of H_{ext}. The explicit dependence of the FMR field H_0 on the field angle θ for a given frequency ω can also be determined. Once the sample parameters are specified, Eqs. (1), (3), (4), and (5), with H_{ext} and ω_0 replaced by H_0 and ω, respectively, can be solved for H_0 as a function of θ.

The FMR analysis also yields an expression for the frequency linewidth, which consists of both L–L and B–B terms;

$$\Delta(\omega/\gamma) = \frac{\lambda}{\gamma M_s}(H_x+H_y) + \frac{1}{\gamma T}. \tag{6}$$

In contrast to the FMR frequency of Eq. (3) which varied as the geometric mean of the stiffness fields, note that the L–L linewidth is proportional to their sum. The B–B contribution to the linewidth, on the other hand, is simply proportional to the B–B relaxation rate and has no dependence on the stiffness fields.

The linewidth given by Eq. (6) is for FMR at a constant external field. When the frequency is held fixed and the field strength is swept, the linewidth is in general much more complicated. One way to determine the field linewidth ΔH from $\Delta(\omega/\gamma)$ is with the approximate relation

$$\Delta H \approx \frac{\partial H_0}{\partial(\omega/\gamma)}\,\Delta(\omega/\gamma). \tag{7}$$

This expression is valid as long as $\Delta\omega \ll \omega$ is satisfied. For a sample with rotational symmetry about the field and magnetization vectors, or in the limit of very large external fields, the derivative in Eq. (7) approaches unity. For other geometries, where the field and magnetization vectors are not aligned, ΔH can exceed $\Delta(\omega/\gamma)$ by an order of magnitude.

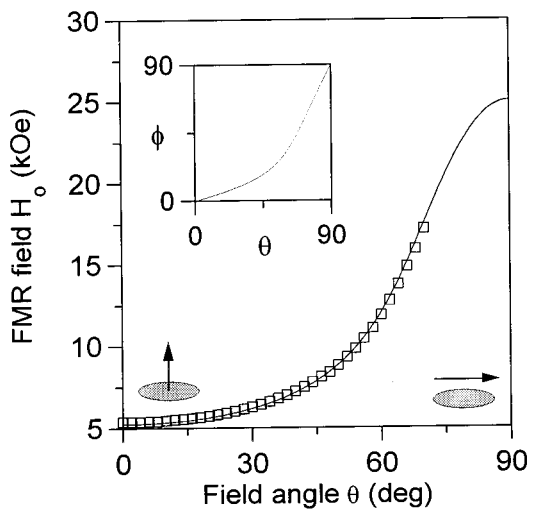

FIG. 2. FMR field H_0 as a function of external field angle θ for the Ba-M disk at a frequency of 50 GHz. The solid curve is based on $\gamma = 2.82$ GHz/kOe, $4\pi M_s = 4.5$ kG, and $H_A = 16.3$ kOe. The inset shows the calculated static magnetization angle ϕ, in degrees, as a function of θ.

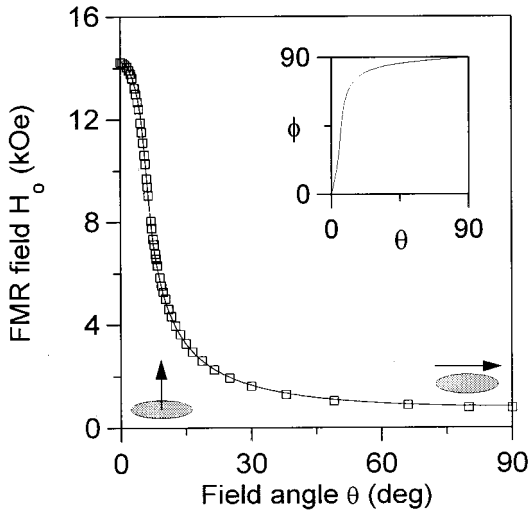

FIG. 3. FMR field H_0 as a function of external field angle θ for the Zn-Y disk at a frequency of 8.8 GHz. The solid curve is based on $\gamma = 2.8$ GHz/kOe, $4\pi M_s = 2.2$ kG, and $H_A = -9.4$ kOe. The inset shows the calculated static magnetization angle ϕ, in degrees, as a function of θ.

This increase is due to a rotation effect, where the magnetization angle ϕ changes as the external field is varied during the FMR experiment.

In addition to the approximate approach of Eq. (7), the field linewidth ΔH can be determined directly from the explicit microwave susceptibility expressions obtained from the uniform mode analysis. Here, a numerical approach is used to find the external field values which correspond to the half power points of the absorption and hence the linewidth. In the limit that $\Delta\omega \ll \omega$ is satisfied, however, the linewidths predicted by the two approaches agree to within several oersteds.

In the following sections, it will prove more convenient to present the linewidth results in terms of their dependence on the magnetization angle ϕ rather than the field angle θ. In the first part of the linewidth analysis, the linewidth ΔH as a function of ϕ for constant L–L damping will be determined from Eqs. (3)–(7) and the stability condition of Eq. (1) and compared to the experimental results. The differences between the experimental linewidths and the L–L predictions will represent the nonintrinsic part of the loss and will be described with the B–B damping. This remaining field linewidth will then be converted to an adjusted frequency linewidth according to Eq. (7). The adjusted linewidth versus magnetization angle can then be compared directly to the $1/\gamma T$ relaxation rates predicted by the two magnon scattering theory.

III. RESULTS

A. FMR field

Figures 2 and 3 show results on the FMR field H_0 versus field orientation angle θ for the Ba-M and Zn-Y samples at 50 and 8.8 GHz, respectively. The squares indicate the data. The solid lines give theoretical predictions to be discussed shortly. The insets show the calculated magnetization angle ϕ as a function of θ.

The variations in H_0 with angle are strikingly different for the two materials. For the easy-axis Ba-M data in Fig. 2, H_0 is small at $\theta = 0°$, with the field along the easy-axis, and large when the field is pulled toward the in-plane orientation at $\theta = 90°$. For the easy-plane Zn-Y data in Fig. 3, H_0 is small at $\theta = 90°$ when the field is in the easy c-plane, and large when the field is pulled to the hard direction at $\theta = 0°$.

The solid lines in the figures represent fits to the data, with $4\pi M_s$ and H_A close to the nominal VSM values. The fits were generated from numerical solution of Eqs. (1), (3), (4), and (5). For the Ba-M case, the curves were based on $\gamma = 2.82$ GHz/kOe, $4\pi M_s = 4.5$ kG, and $H_A = 16.3$ kOe. For the Zn-Y case, the curves were based on $\gamma = 2.8$ GHz/kOe, $4\pi M_s = 2.2$ kG, and $H_A = -9.4$ kOe. The γ values are in good agreement with previous results.[8,9] The values of $4\pi M_s$ and H_A agree to within the experimental error with the VSM results. The good agreement between the experimental H_0 versus θ results and the predicted curves confirms the operational assumption of a uniform mode FMR response.

The calculated ϕ versus θ curves shown in the insets demonstrate another important effect of field orientation. For the Ba-M results in Fig. 2, ϕ is less than or equal to θ over the entire angular range and varies in a relatively smooth manner. This is not the case for the Zn-Y results in Fig. 3, where ϕ is greater than or equal to θ and very small changes in θ give rise to large changes in ϕ near $\theta = 0°$. For even intermediate θ values, however, $\mathbf{M}_s$ is essentially in-plane and ϕ is close to 90°.

The ϕ versus θ results for the Zn-Y disk suggest that the effect of field orientation on FMR should be analyzed in terms of ϕ rather than θ dependences. Moreover, ϕ is the

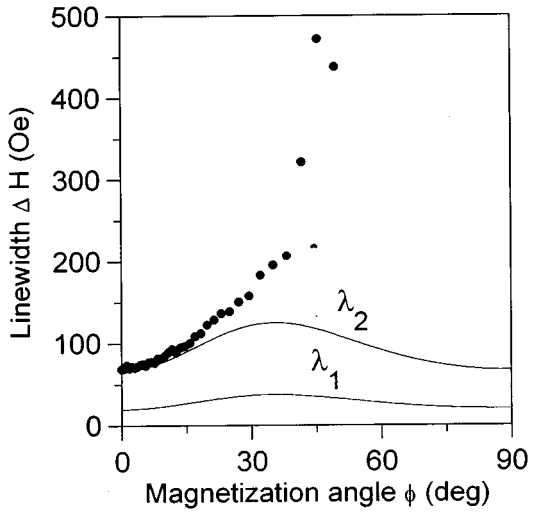

FIG. 4. FMR linewidth ΔH as a function of the static magnetization angle ϕ for the Ba-M disk at 50 GHz. The line indicates the predicted linewidth based on constant Landau–Lifshitz damping with $\lambda_1 = 3.6 \times 10^6$ and $\lambda_2 = 1.2 \times 10^7$ rad/s.

natural independent variable for the calculation of two magnon scattering linewidths because it determines the position of the spin wave manifold in frequency relative to the FMR frequency. For these reasons, the experimental FMR linewidths will be analyzed in terms of their dependence on ϕ rather than θ.

B. FMR linewidth

Figures 4 and 5 show results on the measured FMR linewidth ΔH versus the calculated magnetization angle ϕ for the Ba-M and Zn-Y samples, respectively. The data are represented by the solid circles. The lines in the figures show predicted linewidths based on the L–L damping model. These will be discussed shortly.

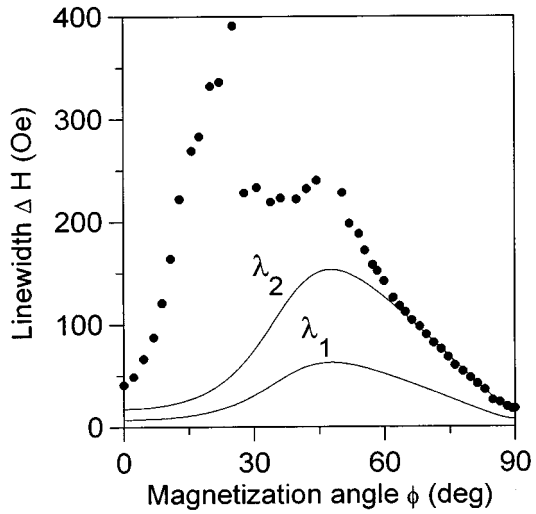

FIG. 5. FMR linewidth ΔH as a function of the static magnetization angle ϕ for the Zn-Y disk at a frequency of 8.8 GHz. The lines show the predicted linewidths based on constant Landau–Lifshitz damping with $\lambda_1 = 3.6 \times 10^6$ rad/s and $\lambda_2 = 8.8 \times 10^6$ rad/s.

The linewidth for the Ba-M disk in Fig. 4 has a minimum value of 69 Oe when the sample is magnetized along the easy axis at $\phi = \theta = 0°$. This linewidth is about twice the value reported by Karim *et al.* at 55 GHz.[1] The linewidth increases and shows a distinct peak at $\phi = 45.4°$ or an external field angle θ of 68°. The maximum measured linewidth is 472 Oe.

For the Zn-Y results of Fig. 5, ΔH increases from 41 Oe for a perpendicular magnetization to a maximum value of 391 Oe at $\phi = 25.2°$, or an external field angle θ of 4.6°. The linewidth then decreases, shows considerable structure, and reaches a minimum value of 18 Oe at the in-plane orientation. Somewhat similar angle dependences for a Mn-doped Zn-Y disk were obtained by Dorsey *et al.*[9]

The lines in Figs. 4 and 5 indicate predicted linewidths for constant values of the L–L relaxation rate λ, based on Eqs. (6) and (7) and the same values of the sample parameters λ, $4\pi M_s$, H_A, and N_Z used for the H_0 versus θ curves of Figs. 2 and 3, respectively. The λ values used for these simulations were $\lambda_1 = 3.6 \times 10^6$ rad/s and $\lambda_2 = 1.2 \times 10^7$ rad/s for the Ba-M and $\lambda_1 = 4.4 \times 10^6$ rad/s and $\lambda_2 = 8.8 \times 10^6$ rad/s for the Zn-Y. These λ value choices will be discussed shortly.

Consider the Ba-M disk results in Fig. 4. The lower of the two L–L curves, designated by λ_1, represents the estimated intrinsic contribution to the linewidth based on effective linewidth measurements of single crystal Mn-doped Ba-M.[1] This λ value yields an out-of-plane linewidth on the order of 20 Oe and a linewidth versus angle curve well below the experimental data. The higher λ_2 curve represents the best fit of the L–L linewidth to the experimental results, where the value of λ was treated as an adjustable parameter. In each case, the L–L linewidth is the same at the $\phi = 0°$ and $\phi = 90°$ limits and shows a small peak at some intermediate angle. The experimental linewidth, however, increases much more rapidly for intermediate values of ϕ.

The rapid increase in linewidth can be attributed to the presence of inhomogeneities and the resulting two magnon scattering loss. As will be discussed in the following section, the two magnon contribution should be a minimum when the magnetization is perpendicular to the disk. In the infinite film limit, the two magnon linewidth should approach zero for this field orientation. As the static field and magnetization vectors are pulled in-plane, the two magnon contribution will increase. For thicker samples, however, the two magnon contribution will not approach zero at the $\phi = \theta = 90°$ limit because a number of spin waves states remain degenerate with the uniform mode. For this reason, the $\lambda_1 = 3.6 \times 10^6$ rad/s value based on effective linewidth measurements will be used to account for the intrinsic loss.

Turn now to the Zn-Y results in Fig. 5. In contrast to the Ba-M results, the experimental linewidths approach a minimum for the in-plane, $\phi = \theta = 90°$ orientation. The lower of the constant L–L curves, which lies well below the experimental points, is for $\lambda_1 = 3.6 \times 10^6$ rad/s, the same estimate used for the Ba-M results in Fig. 4. A fit to the linewidth is

shown by the λ_2 curve. While this approach accounts for the linewidths for $\phi > 60°$, it is clear from a comparison of the data and the two L–L curves that there is an additional contribution to the loss which is dependent upon the orientation of the magnetization vector.

The additional linewidth contribution is again assumed to be a result of two magnon scattering. In that case, the fit of the L–L prediction to the $\phi = 90°$ linewidths shown by the λ_2 curve is inappropriate. As will be discussed shortly, the linewidths near the in-plane orientation should be a result of both two magnon and intrinsic processes. For this reason, the lower estimate of the intrinsic loss parameter, λ_1, will be used.

In order to analyze these effects quantitatively in terms of two magnon scattering, it will be instructive to plot the differences between the experimental and L–L linewidths as a function of ϕ. Moreover, the linewidth differences can be converted to adjusted frequency linewidths $\Delta(\omega/\gamma)$ according to Eq. (7). This approach is useful because the adjusted linewidths can be compared directly with the linewidths $\Delta(\omega/\gamma)_{TM}$ predicted by the two magnon scattering theory.

IV. TWO MAGNON SCATTERING

It is clear from the results in Figs. 4 and 5 that the experimental linewidths cannot be explained in terms of constant L–L damping. The fact that the linewidths show strong angle dependences suggests that the linewidth differences be examined in terms of a two magnon scattering model. For thin disk samples, the two magnon process is strongly dependent on the magnetization angle ϕ.

The angle dependence of the two magnon loss can be understood from an examination of the effect of magnetization orientation on the bulk spin wave manifold for an isotropic thin disk biased to give a fixed FMR frequency ω. The external field H_0 required for FMR for a particular orientation is determined from the uniform mode analysis developed above. Because H_0 will vary with orientation, the frequency of the spin wave manifold will shift as well. Keep in mind that the dispersion relations for uniaxial single crystal materials such as Ba-*M* and Zn-*Y* are much more involved than those for an isotropic sample. The effect of external field orientation on the spin wave manifold and the corresponding two magnon scattering contribution will be considerably more complicated.

Figure 6 shows the bulk spin wave dispersion curves for a thin isotropic disk and different orientations of the external static field for a fixed FMR frequency ω. Diagram (a) is for FMR with the field and static magnetization vectors perpendicular to the disk. Diagram (b) is for FMR at an intermediate field and magnetization angle. Diagram (c) is for FMR with the field and magnetization vectors in-plane. The solid circles represent the FMR frequency, and the shaded strips indicate the degenerate spin wave states at ω.

For case (a) where $\theta = \phi = 0°$ is satisfied, the FMR frequency lies near the bottom of the spin wave manifold and there are few degenerate states. For intermediate angles, as in (b), the band shifts down in frequency and a number of spin wave states have become degenerate. These are the states which can contribute in the two magnon process. For the in-plane configuration in (c) where $\theta = \phi = 90°$ is satisfied, the manifold shifts down in frequency such that the FMR frequency is at the top of the band.

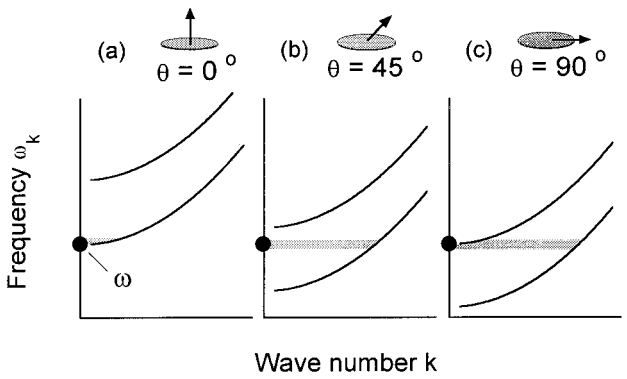

FIG. 6. Schematic illustration of the spin wave manifolds for an isotropic thin disk biased at a fixed FMR frequency and magnetized along three different directions. The solid point indicates the FMR frequency ω. The shaded regions indicate the degenerate spin wave states which may participate in the two magnon scattering process.

It is clear from Fig. 6 that the number of degenerate spin wave states at FMR depends strongly on orientation. For an isotropic material, one would expect the loss associated with the two magnon process to be a minimum for the perpendicular configuration and to increase with angle because there are more degenerate states available for scattering. A more detailed treatment shows that the angle dependence is in fact much more complicated and reflects the size, shape, and number of scattering inhomogeneities. For hexagonal ferrite materials, the anisotropy modifications to the spin wave band influences the angle dependence of the linewidth as well.

The actual two magnon scattering contribution to the loss can be calculated according to a model developed initially by Sparks, Loudon and Kittel (SLK).[3] For a given volume fraction of scattering inhomogeneities of a given size, one can determine the rate at which energy is coupled from the uniform mode to a particular spin wave due to the dipolar interaction between the scatterers and the spin wave. The net relaxation rate is then found from an integration of these rates over all degenerate spin wave states, as indicated by the shaded regions in Fig. 6. The result is an expression for the rate $1/T$ at which energy is coupled out of the uniform precession mode. The two magnon frequency linewidth $\Delta(\omega/\gamma)_{TM}$ is then given by $1/\gamma T$.

In the SLK treatment, the inhomogeneities are modeled as spherical magnetic voids in the sample. The assumption of spherical voids leads to nonisotropic coupling between the uniform precession and the degenerate spin waves. That is, spin waves which propagate in certain directions couple more strongly to the uniform mode than others, due to the geometry of the dipole fields associated with the void. For this reason, calculations were also done for an ''isotropic scattering'' limit in which the coupling is independent of the spin wave propagation direction.

The SLK calculation has been applied previously to the special case of an obliquely magnetized thin film by

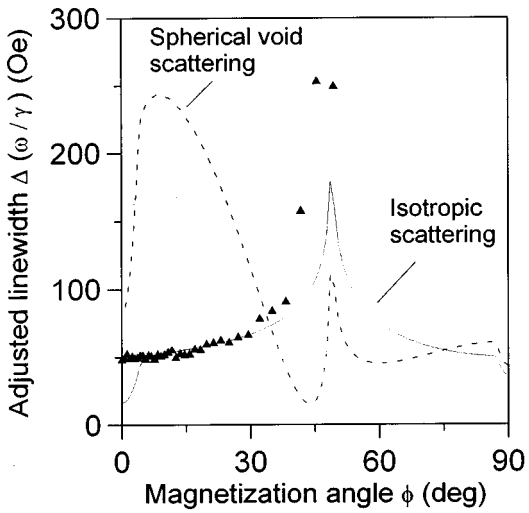

FIG. 7. Adjusted frequency linewidths and predicted two magnon linewidths vs magnetization angle for the Ba-M disk at 50 GHz. The $\Delta(\omega/\gamma)$ values are based on a L–L relaxation rate of 3.6×10^6 rad/s. The lines indicate the predicted $\Delta(\omega/\gamma)_{TM}$ curves for 1 μm radius scatterers and a scatterer-to-sample volume ratio of 0.01.

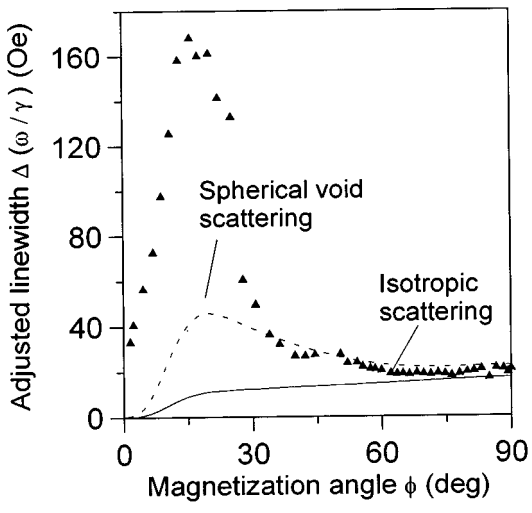

FIG. 8. Adjusted frequency linewidths and predicted two magnon linewidths vs magnetization angle for the Zn-Y disk at 8.8 GHz. The $\Delta(\omega/\gamma)$ values are based on a L–L relaxation rate of 3.6×10^6 rad/s. The lines indicate the predicted $\Delta(\omega/\gamma)_{TM}$ curves for 0.25 μm radius scatterers and a scatterer-to-sample volume ratio of 0.005.

Sparks,[10] but the analysis was restricted to isotropic materials and spherical void scattering. In the present study, it was necessary to extend the treatment to account for the effects of anisotropy on both the FMR conditions and the spin wave dispersion properties. An outline of the two magnon calculation is given in the Appendix. A detailed treatment of the full theory for anisotropic materials will be published elsewhere.

For simplicity, the two magnon linewidth $\Delta(\omega/\gamma)_{TM}$ versus magnetization angle ϕ curves in this work were calculated in the infinite thin film limit. The γ, $4\pi M_S$, and H_A values used in the simulations were the same as those used to calculate the L–L linewidths in Figs. 4 and 5. The exchange constant D in the spin wave dispersion relations is taken to be independent of propagation angle and to have a nominal value of 5×10^{-9} Oe·cm^2/rad^2.

The other two parameters which must be specified are the scatterer radius R and the ratio of total scatterer-to-sample volume p. Here, R and p are both treated as adjustable parameters. As mentioned above, the shape of the $\Delta(\omega/\gamma)_{TM}$ versus ϕ curve can be quite sensitive to the scatterer radius R and the type of scattering interaction. The ratio of scatterer-to-sample volume, p, on the other hand, simply scales the linewidth overall.

Figures 7 and 8 show various calculated frequency linewidths as a function of the static magnetization angle ϕ for the Ba-M and Zn-Y disks, respectively. The triangles indicate the adjusted linewidths determined from the experimental data. These linewidths were calculated by first subtracting the L–L linewidths indicated by the λ_1 curves from the Ba-M and Zn-Y linewidths in Figs. 4 and 5, respectively. The linewidth differences were then converted to frequency linewidths according to Eq. (7). The solid lines show calculated two magnon linewidths based on isotropic scattering. The dashed lines are for spherical void scattering. These curves and their relationship to the data will be discussed shortly.

The angle dependence of the adjusted frequency linewidth for the Ba-M disk in Fig. 7 is qualitatively similar to the field linewidth in Fig. 4, except that it has been shifted down and rescaled. The loss increases steadily from a minimum at the perpendicular orientation with increasing angle to a maximum at $\phi=45°$. The adjusted linewidth for the Zn-Y disk in Fig. 8, on the other hand, shows a very different appearance from the raw linewidths of Fig. 5. The adjusted frequency linewidth shows a sharp maximum at $\phi=16°$ and levels off at larger angles.

It must be stressed that the adjusted linewidths represent the linewidth differences after the estimated L–L contributions have been subtracted off. If the experimental linewidths in Figs. 4 and 5 were described by the L–L predictions, the resulting adjusted linewidths in Figs. 7 and 8 would be zero, independent of angle.

The calculated two magnon frequency linewidths for the Ba-M disk in Fig. 7 are based on the assumption of 1 μm radius voids in the sample and a scatterer-to-sample volume ratio p of 0.01. The choice for this scatterer size was based on previous SEM measurements of 1–3 μm voids in Ba-M single crystals.[4] For the Zn-Y calculation results in Fig. 8, the scatterer radius was 0.25 μm and the scatterer-to-sample volume ratio was 0.005. In this case, both the R and p parameters were chosen by comparing the predicted linewidths to the experimental results and varying their values until reasonable qualitative agreement was found.

Consider the Ba-M results in Fig. 7 first. The isotropic scattering linewidth shown by the solid line is a minimum for $\theta=\phi=0°$, increases rapidly at low angles, and then rises to a distinct peak near $\phi=45°$. The increase in the two magnon linewidth is due to the increase in the number of degenerate spin wave states with increasing angle. The sharp decrease for angles above 45° is a result of the distortion of the

spin wave manifold due to the crystalline anisotropy and the reduction in the number of degenerate spin wave states. The linewidth then sharply drops off at the $\theta=\phi=90°$ limit.

The sharp changes in the isotropic scattering curve near $\theta=\phi=0°$ and $\theta=\phi=90°$ limits is a result of the infinite film approximation used in the calculation. In that case, the uniform mode lies at the bottom of the spin wave manifold for $\phi=0°$, as depicted in diagram (a) of Fig. 6. If only spin waves having a single frequency ω were degenerate, the two magnon linewidth would be zero. However, because there is a finite range of frequencies for the degenerate states, as illustrated by the shaded regions in Fig. 4, the linewidth does reach zero at this limit. At the $\phi=90°$ limit, the effect is similar, and can be understood from a comparison with diagram (c) of Fig. 6.

The sharp variation in the calculated linewidth at the $\theta=\phi=0°$ and $\theta=\phi=90°$ limits would be eliminated if the sample thickness were taken into account. For a noninfinite film, the FMR frequency lies within the spin wave manifold even in the $\theta=\phi=0°$ and $\theta=\phi=90°$ limits, and the linewidth would approach these limit smoothly with a value of about 50 Oe.

The predicted linewidth for spherical void scattering represented by the dashed line in Fig. 7 shows additional structure and much less qualitative agreement with the experimental results, other than the sharp peak near $\phi=45°$. The additional peak near the out-of-plane orientation is a result of the nonisotropic scattering associated with the spherical void model. The experimental data clearly show no such peak, indicating that the coupling between the inhomogeneities and the degenerate spin waves is not mediated by the dipole fields associated with the spherical voids of the SLK theory.

An important consequence of the two magnon scattering model is that the inhomogeneity related linewidth can be minimized in a very thin film sample when the external field is applied out-of-plane. In principle, two magnon scattering could be eliminated even for thin films with significant microstructure.

Turn now to the Zn-*Y* results and two magnon predictions in Fig. 8. As with the Ba-*M* results, a comparison of the adjusted linewidths based on measured values and these theoretical curves generally supports the hypothesis of two magnon scattering loss. The main feature of the adjusted linewidths is the large peak at $\phi=16°$. Compare the adjusted linewidths with the predictions for isotropic two magnon scattering. In this limit, the two magnon linewidth simply increases with angle and shows no sharp maximum or peak, regardless of the scatterer size.

The two magnon scattering linewidth for spherical void scattering shown by the dashed line shows a clear peak. For scatterer radii in the range of 0.2–0.4 μm, this peak occurs roughly at the same ϕ value as the maximum in the adjusted linewidths. Keep in mind that the physical origin of this peak is a result of the spherical void scattering model and the nonisotropic coupling between the void and the scatterer. The sharp peak in the Ba-*M*, on the other hand, was due to the change in the density of degenerate states due to the anisotropic warping of the spin wave manifold.

The Zn-*Y* results are in contrast to those for the Ba-*M* sample. For the easy-axis Ba-*M* disk, the isotropic two magnon scattering calculation gave better qualitative agreement with the experimental linewidths. For the Zn-*Y* sample, the assumption of spherical voids was necessary in order to account for the linewidth peak. In both cases, it should be kept in mind that the particular *p* parameters used for the fits depend on the λ values used to determine the adjusted linewidths and are only estimates of the inhomogeneity-to-sample volume ratio.

There are a number of additional considerations which may be important in the two magnon calculation but have been neglected in this analysis. First, the exchange constant *D* has been taken to be independent of propagation angle. This may not be the case for highly anisotropic single crystal Ba-*M* and Zn-*Y* hexagonal ferrite materials.[11] An exchange constant which depends on propagation direction leads to further distortion of the spin wave manifold and hence modifies the number of degenerate spin waves states for a given field orientation. Second, the effect of the ellipticity of the uniform mode and the spin waves has also been neglected. It is reasonable to expect that the ellipticity would influence the coupling between the inhomogeneities and the degenerate spin waves. For example, the coupling between a circularly precessing uniform mode would be stronger to a circularly, rather than elliptically, precessing spin wave. Because the ellipticities of the uniform mode and spin waves depend on the orientation and magnitude of the external field, the overall angle dependence of the linewidth will be modified as well. Third, because the effective anisotropy fields are so large in typical hexagonal ferrite materials, a scattering Hamiltonian based on fluctuations in H_A rather than $4\pi M_s$ may provide a better model of the two magnon interaction.

V. CONCLUSION

In this work, the FMR field and half-power linewidths were measured as a function of the external field angle for single crystal Ba-*M* and Zn-*Y* hexagonal ferrite *c*-plane disks. The FMR field versus angle results showed good agreement with the predictions of a uniform mode analysis. The experimental FMR linewidths were first compared to the predicted linewidths based on constant L–L damping. This approach, however, could not account for the observed angle dependences.

The linewidth differences were then converted to adjusted frequency linewidths and compared with the predictions for two magnon scattering relaxation based on the Sparks, Loudon, and Kittel theory. In both cases, the two magnon model gave some qualitative explanation for the observed angle dependences. For the Ba-*M* sample, the two magnon fit was based on isotropic scattering, 1 μm radius inhomogeneities, and a scatterer-to-sample volume ratio of 0.01. This scatterer size is on the order of the typical voids observed in single crystal Ba-*M* materials with SEM measurements. For the Zn-*Y* sample, the two magnon fit was based on spherical void scattering, 0.25 μm radius inhomogeneities, and a scatterer-to-sample volume ratio of 0.005.

ACKNOWLEDGMENTS

The authors acknowledge Dr. P. Kabos, Dr. B. A. Kalinikos, and R. Cox for helpful discussions during the course of this study. This work was supported, in part, by the United States Office of Naval Research (ONR) Grants N00014-94-1-0096 and N00014-91-J-1324. The samples were prepared at Purdue University, West Lafayette, Indiana, by Dr. M. A. Wittenauer under ONR Grant N00014-91-J-1323.

APPENDIX: TWO MAGNON CALCULATION

This Appendix describes an explicit method for the calculation of the two magnon linewidth $\Delta(\omega/\gamma)_{TM}$ as a function of the magnetization angle ϕ. The approach is based on the original SLK theory applied to the special case of an infinite, anisotropic disk with the c-axis normal to the disk plane. The new features here are: (1) the use of the full anisotropic dispersion relations, (2) an isotropic scattering model which accounts for nonspherical scattering inhomogeneities, and (3) a finite frequency range for the degenerate spin waves on the order of the intrinsic frequency linewidth.

As discussed above, the frequency linewidth for two magnon scattering is equivalent to the rate at which energy is coupled from the uniform mode to degenerate spin waves.[7] In terms of field units, the frequency linewidth is given by $\Delta(\omega/\gamma)_{TM}=1/\gamma T$, where T is the decay time for the energy associated with the precessing magnetization. In many treatments, T is the relaxation time associated with the magnitude of the dynamic magnetization itself, resulting in a frequency linewidth of $2/\gamma T$.[12]

The SLK calculation yields the rate at which energy is coupled from the uniform mode to a given spin wave with frequency ω_k and wave vector $\mathbf{k}$ due to the dipolar interaction between the scatterer and the spin wave. The orientation of $\mathbf{k}$ is specified by the polar angle θ_k between the wave vector and the static magnetization and an azimuthal angle ϕ_k which is taken to be zero for projections along the X-axis depicted in Fig. 1. The resulting frequency linewidth is proportional to the net rate and can be expressed in terms of a triple integral in k-space,

$$\Delta(\omega/\gamma)_{TM}=\frac{6p\gamma(4\pi M_s)^2R^3}{\pi\Delta\omega_i}\times\int_0^{\infty}\int_{f(k)}^{\pi/2}\int_{a(k,\phi_k)}^{b(k,\phi_k)}\left[(3\cos^2\theta_k-1)\frac{j_t(kR)}{kR}\right]^2\times d(\cos\theta_k)\,d\phi_k k^2\,dk. \tag{A1}$$

The limits of the $\cos\sigma_k$ integral, $a(k,\phi_k)$ and $b(k,\phi_k)$, are given by

$a(k,\phi_k)$

$$=\begin{cases}1 & \omega+\dfrac{\Delta\omega_i}{2}<\omega_{\min}\\ \sqrt{\dfrac{\omega_{\max}^2-\left(\omega+\dfrac{\Delta\omega_i}{2}\right)^2}{\omega_{\max}^2-\omega_{\min}^2}} & \omega_{\min}<\omega+\dfrac{\Delta\omega_i}{2}<\omega_{\max}\\ 0 & \omega+\dfrac{\Delta\omega_i}{2}>\omega_{\max}\end{cases} \tag{A2}$$

and

$b(k,\phi_k)$

$$=\begin{cases}1 & \omega-\dfrac{\Delta\omega_i}{2}<\omega_{\min}\\ \sqrt{\dfrac{\omega_{\max}^2-\left(\omega-\dfrac{\Delta\omega_i}{2}\right)^2}{\omega_{\max}^2-\omega_{\min}^2}} & \omega_{\min}<\omega-\dfrac{\Delta\omega_i}{2}<\omega_{\max},\\ 0 & \omega-\dfrac{\Delta\omega_i}{2}>\omega_{\max}\end{cases} \tag{A3}$$

where $\Delta\omega_i$ is the intrinsic frequency linewidth, $\omega_{\max}$ is the spin wave frequency at the top of the manifold where $\theta_k=90°$, given by

$$\omega_{\max}^2=\gamma^2(H_i+Dk^2)(H_i+Dk^2-H_A\sin^2\phi)+\gamma^2 4\pi M_s(H_i+Dk^2-H_A\sin^2\phi\cos^2\phi_k), \tag{A4}$$

and $\omega_{\min}$ is the spin wave frequency at the bottom of the manifold where $\theta_k=0°$, given by

$$\omega_{\min}^2=\gamma^2(H_i+Dk^2)(H_i+Dk^2-H_A\sin^2\phi). \tag{A5}$$

The parameter H_i is the effective internal static magnetic field, which for an infinite thin film obeys

$$\omega^2=\gamma^2H_i[H_i+(4\pi M_s-H_A)\sin^2\phi]. \tag{A6}$$

The ϕ_k limit denoted $f(k)$ is also related to the anisotropic spin wave dispersion relations. For an isotropic material, where $H_A=0$, $f(k)$ is always zero. In an anisotropic material, depending on the field orientation and material parameters, this limit may range between zero and $\pi/2$ and obeys

$$\cos^2[f(k)]=\frac{\gamma^2(H_i+Dk^2)(H_i+Dk^2-H_A\sin^2\phi+4\pi M_s)-\omega^2}{4\pi M_s\gamma^2H_A\sin^2\phi} \tag{A7}$$

provided that the right-hand side is less than or equal to one. Otherwise, $f(k)$ is equal to zero. This term accounts for the anisotropic distortion of the manifold and the reduction in degenerate states.

The bracketed term in the integrand of Eq. (A1) characterizes the coupling between the uniform mode and a spin wave of wave vector $\mathbf{k}$ and holds only for spherical void

scattering. For isotropic scattering, the $(3\cos^2\theta_k-1)^2$ term is replaced by a constant. The $j_1(kR)$ term is the first spherical Bessel function.

The dependence on the intrinsic frequency linewidth $\Delta\omega_i$ can be understood as follows. In the original SLK treatment, only spin waves at the operating frequency ω are included in the calculation. This restriction can be accounted for in the linewidth expression with a Dirac delta function $\delta(\omega_k-\omega)$.[3] Because of the subsequent relaxation of the degenerate spin waves, however, which is characterized by a linewidth on the order of $\Delta\omega_i$, spin wave states in the range $\omega\pm\Delta\omega_i/2$ can participate in two magnon scattering. This range was illustrated schematically in Fig. 6 by the shaded bands representing the set of degenerate spin waves. The $\Delta\omega_i$ values used were 56 and 20 MHz for the Ba-*M* and Zn-*Y* cases, respectively, and were based on the intrinsic linewidths corresponding to the λ_1 curves in Figs. 4 and 5.

In order to obtain Eq. (A1), the delta function of the SLK theory was replaced by a function of width $\Delta\omega_i$ and height $1/\Delta\omega_i$. As can be seen from Eqs. (A2) and (A3), the $a(k,\phi_k)$ and $b(k,\phi_k)$ limits are related to the width $\Delta\omega_p$ while the $1/\Delta\omega_i$ dependence is reflected in the prefactor of Eq. (A1). So long as $\Delta\omega_i\ll\omega$ is satisfied, the two magnon linewidth is essentially independent of $\Delta\omega_i$.

The integrand of Eq. (A1) reflects the assumption of spherical scatterers through the $(3\cos^2\theta_k-1)^2$ term. This term accounts for the fact that spin waves which propagate in particular directions will couple to a spherical scatterer more strongly than others. As a result, the assumption of spherical inhomogeneities will give rise to characteristic dependences in the $\Delta(\omega/\gamma)_{TM}$ versus ϕ curve. The overall angle dependence will reflect both the density of degenerate states and the directional dependent coupling. It is useful, therefore, to also consider the angle dependence for nonspherical scatterers, where the angular coupling term $(3\cos^2\theta_k-1)^2$ with its average value, which is 0.8. This approach is designated ''isotropic scattering.''

The $[j_1(kR)/kR]^2$ term, which has a value of 1/9 for $kR=0$ and is essentially zero for $kR>\pi$, ensures that the spin waves involved in the two magnon process have wavelengths on the order of the scatterer size or larger. For large inhomogeneities, only spin waves with low wave numbers can contribute in the scattering process. For smaller inhomogeneities, higher wave number spin waves can participate as well. As a result, the size of the scattering inhomogeneities can have a significant effect on the shape of the $\Delta(\omega/\gamma)_{TM}$ versus ϕ curve.

In order to calculate the two magnon scattering linewidth as a function of the magnetization angle ϕ, Eq. (A1) must be evaluated numerically over the entire range of ϕ values. The first step is to determine the effective internal static magnetic field H_i at a given ϕ according to Eq. (A6).

The first integral to be performed is over the $\cos\theta_k$ variable. The limits of the $\cos\theta_k$ integral are due to the restriction that only those states which lie within $\pm\Delta\omega_i/2$ of the operating frequency ω can participate in the two magnon process. The function $a(k,\phi_k)$ is derived from the anisotropic spin wave dispersion relation and is equivalent to $\cos\theta_k$ when $\omega_k=\omega+\Delta\omega_i/2$. The function $b(k,\theta_k)$ is equivalent to $\cos\theta_k$ for $\omega_k=\omega-\Delta\omega_i/2$.

The second integration involves the azimuthal angle ϕ_k. For an isotropic material, the lower limit of this integral, $f(k)$, is always zero. Because of the anisotropy however, the dispersion manifold can become distorted such that a number of states are reduced in frequency and are no longer degenerate. The $f(k)$ function accounts for this effect on the degeneracy.

The third and final integration is over the wave number k. In practice, the upper limit can be replaced by π/R, as the spherical Bessel function expression in the integrand is negligible for larger k values. In this manner, the linewidth expression of Eq. (A1) can be evaluated over the entire range of magnetization angles in order to generate the $\Delta(\omega/\gamma)_{TM}$ versus ϕ curves, such as those shown in Figs. 7 and 8.

[1] R. Karim, S. D. Ball, J. R. Truedson, and C. E. Patton, J. Appl. Phys. **73**, 4512 (1993).
[2] M. J. Hurben and C. E. Patton, Digests of the INTERMAG'95 Conference, JC-03, San Antonio, April 1995 (unpublished).
[3] M. Sparks, R. Loudon, and C. Kittel, Phys. Rev. **122**, 791 (1961).
[4] M. A. Wittenauer, J. A. Nyenhuis, A. I. Schindler, H. Sato, F. J. Friedlander, J. R. Truedson, R. Karim, and C. E. Patton, J. Cryst. Growth **130**, 553 (1993).
[5] J. A. Osborn, Phys. Rev. **67**, 351 (1945).
[6] I. Bady, IEEE Trans. Magn. **3**, 521 (1967).
[7] M. Sparks, *Ferromagnetic Relaxation Theory* (McGraw-Hill, New York, 1964).
[8] W. H. von Aulock, *Handbook of Microwave Ferrite Materials* (Academic, New York, 1965).
[9] P. Dorsey, K. Sun, C. Vittoria, M. A. Wittenauer, F. J. Friedlander, and A. Schindler, J. Appl. Phys. **67**, 5524 (1990).
[10] M. Sparks, Phys. Rev. **1**, 3856 (1970).
[11] E. Schlömann, R. I. Joseph, and I. Bady, J. Appl. Phys. **34**, 672 (1963).
[12] See, for example, V. Kambersky and C. E. Patton, Phys. Rev. B **11**, 2668 (1975).